Stationarity Analysis of V2I Radio Channel in a Suburban Environment

Marwan Yusuf, Emmeric Tanghe, Frédéric Challita, Pierre Laly, Davy P. Gaillot, Martine Liénard, Luc Martens, and Wout Joseph

***Abstract*—Due to rapid changes in the environment, vehicular communication channels no longer satisfy the assumption of wide-sense stationary uncorrelated scattering. The non-stationary fading process can be characterized by assuming local stationarity regions with finite extent in time and frequency. The local scattering function (LSF) and channel correlation function (CCF) provide a framework to characterize the mean power and correlation of the non-stationary channel scatterers, respectively. In this work, we estimate the LSF and CCF from measurements collected in a vehicle-to-infrastructure radio channel sounding campaign in a suburban environment in Lille, France. Based on the CCF, the stationarity region is evaluated in time as 567 ms, and used to capture the non-stationary fading parameters. We obtain the time-varying delay and Doppler power profiles from the LSF, and we analyze the corresponding root-mean-square (RMS) delay and Doppler spreads. We show that the distribution of these parameters follows a lognormal model. Finally, application relevance in terms of channel capacity and diversity techniques is discussed. Results show that the assumption of ergodic capacity and the performance of various diversity techniques depend on the stationarity and coherence parameters of the channel. The evaluation and statistical modeling of such parameters can provide a way of tracking channel variation, hence, increasing the performance of adaptive schemes.**

***Index Terms*—vehicular, propagation model, measurement, stationarity, fading, delay, Doppler, scattering function, correlation function, suburban.**

I. Introduction

VEHICULAR communications have recently attracted much interest due to the rapid development of wireless communication technologies. Through the integration of information and communication technologies, all road users can gather sensor data and share information about traffic and road state dynamics with each other and with the road infrastructure. This envisioned intelligent transportation system (ITS) will improve the safety and efficiency of transportation by enabling a wide range of applications [1]. Such systems require reliable low-latency vehicular-to-vehicular (V2V) and vehicular-to-infrastructure (V2I) communication links that provide robust connectivity at a fair data rate. An essential requirement for the development of such vehicular systems is the accurate modeling of the propagation channel in different scenarios and environments [2].

This research was supported by the VLAIO project "Smart Highway" and the EOS project "Multi-service Wireless Network (MUSE-WINET)".

Marwan Yusuf, Emmeric Tanghe, Luc Martens and Wout Joseph are with the Department of Information Technology, IMEC-WAVES, Ghent University, Belgium (e-mail: marwan.yusuf@ugent.be, emmeric.tanghe@ugent.be)

Frederic Challita, Pierre Laly, Davy P. Gaillot and Martine Liénard are with the Electronics Department, IEMN-TELICE, University of Lille, France.

Manuscript received XXX, XX, 2019; revised XXX, XX, 2019.

Some V2I propagation channels resemble existing cellular links, where one node is stationary, while the other node is mobile. However, the placement height and surroundings of the infrastructure nodes for vehicular communication are unique, resulting in different dominant propagation mechanisms [3]. In urban areas, the roadside unit (RSU) is placed at lamppost height much lower than the rooftops of surrounding buildings, typically at intersections. In other areas, the RSU is placed at 1-2 m height, making it similar to the V2V scenario from a propagation point of view [3]. Owing to the changing scattering environment and the mobility of the transmitter (Tx) or the receiver (Rx), the vehicular communication channel is characterized by a non-stationary fading process [4], [5]. Depending on the relative speed of scatterers, the non-stationarity of V2I and V2V channels need not to be identical. One of the main challenges of V2I is the expected large Doppler shift of the line-of-sight (LOS) path when the vehicle passes by the RSU at high speed. While this may happen in few V2V cases (e.g. overtaking a slower vehicle or vehicles traveling in opposite directions) [6], it is generally more persistent in the V2I scenario compared to V2V scenarios where vehicles are traveling in the same direction. Such fast Doppler shifts would increase the non-stationarity of the channel and cause serious performance degradation to the communication system, if not carefully addressed via Doppler planning and compensation [7].

In the past, propagation channel models have adopted the wide-sense stationarity (WSS) uncorrelated scattering (US) assumptions [8]. The WSSUS assumptions imply that second-order channel statistics are independent of time and frequency, and hence, allow for a simplified statistical description of channels; this has formed the basis of many designs of wireless transceivers. However, the WSSUS assumptions are not always fulfilled in practice, particularly in vehicular scenarios. Hence, this must be accounted for [9]. The author in [10] has shown that, in both single and multi-carrier systems, the WSS assumption in V2V channels can lead to optimistic bit-error-rate simulation results that are erroneous. In reality, power, delay and Doppler associated with reflected multipath components (MPC) drift with time (WSS-violation), and channels show correlated scattering due to several MPCs that are close in the delay-Doppler domain resulting from the same physical object, or delay/Doppler leakage due to bandwidth/time limitations at Tx or Rx (US-violation). In the literature, various approaches have been proposed to overcome these limitations: 1) different tap models depending on the delay spread and the bit error rate statistics [9], 2) "birth/death" Markov process to

account for the appearance and disappearance of taps [11], 3) stochastic modeling of the dynamic scatterers evolution and their delay and angular properties [12] or 4) geometry-based channel modeling (GSCM) that includes inherently the non-stationary behavior of the channel via the dynamic nature of the scattering environment geometry [13], [14]. In order to evaluate how much these models truly reflect the varying nature of the vehicular channel, accurate characterization of the non-stationarity of the channel is required.

The non-stationary fading process of vehicular channels can be characterized by assuming local stationarity for a finite region in time and frequency. A definition of the stationarity time and stationarity bandwidth are proposed in [5], where the author provides a theoretical framework that extends the scattering function of the WSSUS to a time-frequency (TF) dependent local scattering function (LSF). The LSF can be estimated within this finite region where WSSUS assumptions approximately hold [15]. This stationarity region is computed from the channel correlation function (CCF), which extends the TF correlation function of the WSSUS [5], [8].

A. Related Work

For a non-stationary channel, the fading statistics change in time. Since communication algorithms often rely on the knowledge of second-order statistics of the channel, appropriate measures of the similarity between channel statistics are required, so that the fading parameters can be accurately evaluated and the channel modeling becomes physically meaningful. For stochastic modeling [12], the WSS region is first estimated and the time-varying parameters (MPCs lifetime, birth, initial power, angle and delay as well as their dynamic evolution) are modeled in terms of the WSS regions, while the small-scale fading is characterized within each region. GSCM can incorporate non-stationarity via varying some channel parameters over time (e.g. number of delay taps and angles of propagation paths of regular-shaped GSCM in [13]), or via random mobility models that use dynamic motion (e.g. changes of speed and moving direction in [14]). The WSS region is then used as a measure of non-stationarity in order to validate such models, by showing that the resulting channel transfer function has the same WSS region as found from realistic measurements [13]. Several measurement-based metrics have been proposed to measure the size of the WSS region.

A traditional measure of the change in channel statistics is the shadow fading correlation [16], where the decorrelation distance of shadowing can be considered as an equivalent stationarity distance as proposed in [17]. Correlation matrix distance (CMD) was proposed in [18], [19] to characterize the non-WSS behavior of MIMO channels. Spectral divergence (SD) measures the distance between strictly positive spectral densities and was applied to LSF measured at different times in [20]. However, since it is an unbounded pseudo-metric, it can only qualitatively assess the non-WSS nature of channels. A comparison of the above metrics was provided in [21], where it was suggested to use SD and shadowing metrics for a measurement system with a small electrical array aperture, e.g. 4×4, and to use the CMD metric for arrays with large electrical apertures. Authors in [22], [23] defined a statistical test where the intervals of WSS are identified based on the evolutionary power delay profile (PDP) estimated at different time instances. Another approach is based on the collinearity between spectral densities. Collinearity was calculated between consecutive PDPs in [24] and between LSFs in [25], and the support of the region where it exceeds a certain threshold was used as an estimate of the local stationarity region. Based on the results in [4], the same authors characterize the RMS delay and Doppler spreads of non-WSS channels in [26], where they use a bimodal Gaussian mixture to model their statistical distribution. Other papers show the distribution of the spreads to follow a lognormal model [27]–[30]

While these metrics manage to capture the non-WSS behavior of the channel, they are mainly empirical measures; they lack a theoretical framework that can be used as an extension to the WSSUS in [8]. In addition, many of the existing works have limitations, e.g. dependency on the spatial structure of the MIMO channel which is not valid for single antenna systems, and measurements in cellular scenarios that are different from vehicular scenarios.

B. Contribution of This Paper

In our work, we investigate the stationarity of a V2I channel measured in a suburban environment in Lille, France, using the framework proposed in [5]. According to [4], the observed fading process in vehicular channels shows a much stronger violation of the WSS assumption than the US, keeping in mind that violations of the WSS assumption do not necessarily imply violations of the US. Hence, we investigate the stationarity region in time based on the CCF introduced in [5], and compare it to the empirical measure of collinearity. Then, we statistically model the delay and Doppler spreads of the channel across stationarity regions. To completely characterize such doubly dispersive channels, the values of the coherence region are obtained and used to investigate some system design relevance, e.g. the effect of non-stationarity on the assumption of ergodic capacity and effective diversity [31]. The novelty of this paper is the following:

- Evaluating the stationarity time using the channel correlation function and comparing it with the empirical collinearity method
- Statistically modeling the RMS delay and Doppler spreads across several regions of stationarity
- Investigating the practical relevance of the non-stationary channel in terms of the ergodic assumption and effective diversity

C. Paper Outline

The measurement setup and scenario are introduced in Section II. In Section III, we describe the CCF, and based on it we define the stationary time and the channel parameters under consideration. The measured data and the performed pre-processing are discussed in Section IV. The full characterization of the stationarity region and channel parameters are presented in Section V. We draw conclusions in Section VI.

Fig. 1. Tx as a roadside unit (left) and the omnidirectional antenna used at both Tx and Rx (right)

TABLE I
MIMOSA CHANNEL SOUNDER CONFIGURATION

Parameter	Setting
center frequency	1.35 GHz
bandwidth	50 MHz
Tx and Rx antennas	omni 0.8-6.0 GHz
Tx and Rx polarization	vertical
OFDM symbol duration T_S	81.92 μs
cyclic prefix duration T_{CP}	$0 \leq T_{CP} \leq T_S$
channel acquisition time	$2\,(T_S + T_{CP}) \leq 327.68$ μs
total recording time	48.3 s

II. Measurement Setup and Scenario

Channel measurements are performed with the Multi-input Multi-output System Acquisition (MIMOSA) radio channel sounder [32]. We use 50 MHz of transmission bandwidth centered around a carrier frequency of 1.35 GHz. This carrier frequency lies conveniently within the operating band of the LTE-V standard [33] radio interface that supports V2I communications (named Uu-interface), which operates in the licensed 2 GHz band (880-2690 MHz). For this measurement campaign, a single wideband omnidirectional antenna is used at both Tx and Rx for the sounding signal, while we add 6 patch antennas at Rx just for synchronization and detection enhancement. The data from the Tx antenna is modulated onto the carrier using orthogonal frequency division multiplexing (OFDM). Table I summarizes the technical configuration of the MIMOSA channel sounder used for this measurement campaign.

Measurements have been carried out at the campus of the university of Lille in France. The environment can be categorized as suburban: the road is narrow with one lane in each direction and buildings and vegetation are set back 5-8 m from the curb. In order to follow the V2I scenario, the Tx is placed on the curb with the antenna at 2.5 m height, as shown in Fig. 1. The Rx antenna is mounted on the rooftop of the van carrying the Rx inside. The van moves along the road at 40 km/h speed, crossing Tx position during a total route of 500 m shown in Fig. 2. Due to storage limitations of

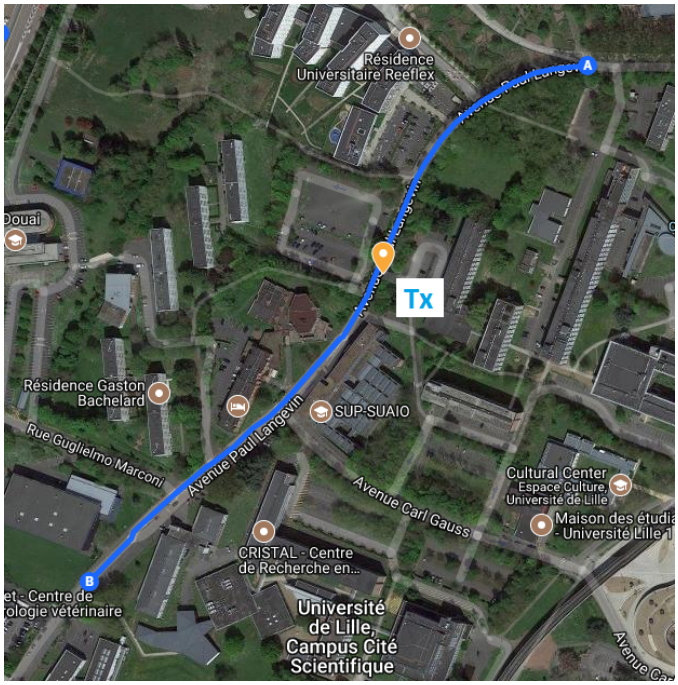

Fig. 2. Top view of measurement route at the university of Lille campus. Tx location is marked with a yellow pin and Rx van moves from point B to A (Map data ©2018 Google).

the channel sounder, we obtain a snapshot repetition time t_s = 975.3 μs. With this parameters setting, we capture a total number of snapshots X = 49536 snapshots, each with 512 samples in frequency domain, and we achieve a maximum Doppler shift of $1/2t_s$ = 512 Hz and a minimum resolvable delay resolution of 20 ns.

III. Stationarity Assessment

For WSSUS channels, the scattering function is the power spectrum of the channel transfer function (CTF), while for non-WSSUS channels, the scattering function is not defined [8]. In [5], the author introduces the TF-dependent LSF as an extension to the WSSUS scattering function. The CCF appropriate for the non-WSSUS case is also defined, which extends the TF correlation function of WSSUS channels. The LSF $C_{\mathbf{TF}}$ and CCF $A_{\mathbf{TF}}$ are given as

$$C_{\mathbf{TF}}(t,f,\tau,\upsilon) = \iint R_{\mathbf{TF}}(t,f,\Delta t,\Delta f)\mathrm{e}^{-j2\pi(\upsilon\Delta t-\tau\Delta f)}\mathrm{d}\Delta t\mathrm{d}\Delta f \tag{1}$$

and

$$A_{\mathbf{TF}}(\Delta t,\Delta f,\Delta\tau,\Delta\upsilon) = \iint R_{\mathbf{TF}}(t,f,\Delta t,\Delta f)\mathrm{e}^{-j2\pi(t\Delta\upsilon-f\Delta\tau)}\mathrm{d}t\mathrm{d}f \tag{2}$$

where $R_{\mathbf{TF}}(t,f,\Delta t,\Delta f)$ is the autocorrelation of the CTF for time lag Δt and frequency lag Δf. It is shown in [5] that the LSF describes the mean power of effective scatterers causing delay-Doppler shifts (τ,υ) at time t, and frequency f. However, it does not characterize the scatterers correlation, thus the introduction of CCF. The following relation

shows that the correlation of scatterers separated by the lags $(\Delta\tau, \Delta\upsilon, \Delta t, \Delta f)$ is measured by the integral CCF

$$A_{\mathbf{TF}}(\Delta t, \Delta f, \Delta\tau, \Delta\upsilon) = \iiiint C_{\mathbf{TF}}(t, f, \tau, \upsilon) \mathrm{e}^{-j2\pi(t\Delta\upsilon - f\Delta\tau + \tau\Delta f - \upsilon\Delta t)} \mathrm{d}t\mathrm{d}f\mathrm{d}\tau\mathrm{d}\upsilon \tag{3}$$

A. Stationarity Region

The channel's non-stationarity in the TF domain corresponds to the delay-Doppler correlations in the dual domain (i.e. to the CCF spread in $(\Delta\tau, \Delta\upsilon)$ directions), as shown in (3). The CCF spread about the origin can be measured by the following moment of the CCF

$$s_{\mathbf{TF}}^{(w)} = \frac{1}{\|A_{\mathbf{TF}}\|_1} \iiiint |w| \; |A_{\mathbf{TF}}(\Delta t, \Delta f, \Delta\tau, \Delta\upsilon)| \times \mathrm{d}\Delta t\mathrm{d}\Delta f\mathrm{d}\Delta\tau\mathrm{d}\Delta\upsilon \tag{4}$$

where $\|A_{\mathbf{TF}}\|_1$ is the first norm of the CCF across all four dimensions. Setting the weight factor w to $\Delta\upsilon$ and $\Delta\tau$ results in the CCF moments $s_{\mathbf{TF}}^{(\Delta\upsilon)}$ and $s_{\mathbf{TF}}^{(\Delta\tau)}$, respectively. These moments quantify the Doppler and delay lag spans within which there are significant correlations. Hence, the stationarity region can be defined via a stationarity time and a stationarity bandwidth, respectively, as follows

$$T_s = \frac{1}{s_{\mathbf{TF}}^{(\Delta\upsilon)}}, \qquad F_s = \frac{1}{s_{\mathbf{TF}}^{(\Delta\tau)}}. \tag{5}$$

According to [5], the channel can be approximated with good accuracy by a WSSUS channel within this region. Hence, the stationarity region can be used to meaningfully evaluate the fading parameters and their statistics.

B. Channel Parameters

The amount of delay and Doppler spread is determined by the extension of the TF-varying LSF in (τ,υ) directions. Since the LSF only changes significantly from one stationarity region to another, we calculate the (local) TF-dependent RMS delay spread σ_τ and RMS doppler spread σ_υ within each region as

$$\sigma_\tau^2(t,f) = \frac{1}{\rho_{\mathbf{TF}}^2(t,f)} \int (\tau - \overline{\tau})^2 \; P_{\mathbf{TF}}(t,f,\tau) \; \mathrm{d}\tau$$
$$\sigma_\upsilon^2(t,f) = \frac{1}{\rho_{\mathbf{TF}}^2(t,f)} \int (\upsilon - \overline{\upsilon})^2 \; Q_{\mathbf{TF}}(t,f,\upsilon) \; \mathrm{d}\upsilon \tag{6}$$

where $\rho_{\mathbf{TF}}^2(t,f) = \iint C_{\mathbf{TF}}(t,f,\tau,\upsilon)\mathrm{d}\tau\mathrm{d}\upsilon = \mathrm{E}\{|H(t,f)|^2\}$ is the local path gain, $P_{\mathbf{TF}}(t,f,\tau) = \int C_{\mathbf{TF}}(t,f,\tau,\upsilon)\mathrm{d}\upsilon$ is the local PDP, $Q_{\mathbf{TF}}(t,f,\upsilon) = \int C_{\mathbf{TF}}(t,f,\tau,\upsilon)\mathrm{d}\tau$ is the local Doppler power profile (DPP), and $\overline{\tau}$ and $\overline{\upsilon}$ are the local mean delay and Doppler, respectively.

A measure of the channel selectivity is the coherence region, which quantifies the time and frequency spans within which the CTF is considered constant, or at least strongly correlated. The coherence region is defined by a coherence time T_c and a coherence bandwidth F_c that can be approximately related to the delay and Doppler spreads as follows [34]:

$$T_c = \frac{1}{2\pi\sigma_\upsilon}, \qquad F_c = \frac{1}{2\pi\sigma_\tau}. \tag{7}$$

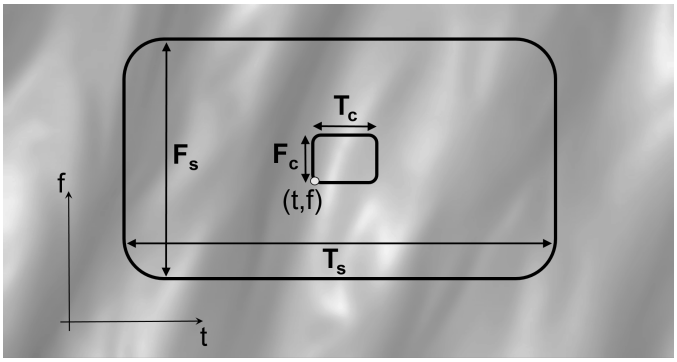

Fig. 3. Illustration of the coherence region (T_c, F_c) and stationarity region (T_s, F_s) at a certain point (t,f) in the TF domain. The background represents the magnitude of the CTF in grayscale.

The relation between the stationarity region and coherence region is of great importance. According to [15], the LSF of non-WSSUS channels can be considered a TF-dependent delay-Doppler power spectrum only if the channel is both dispersion-underspread and correlation-underspread. These two underspreads constitute the doubly-underspread (DU) property. A simple way of describing this property is using the following inequality

$$T_s F_s \gg T_c F_c \gg 1 \tag{8}$$

which states that: the CTF is slowly varying (dispersion-underspread), and the channel statistics variation is even slower (correlation-underspread). Thus, the stationarity region is much larger than the coherence region for DU channels. An illustration of a DU channel is shown in Fig. 3 and further practical implications are discussed in Section V.

IV. Measured Data and Pre-processing

Due to the high mobility of Tx, Rx and scatterers in vehicular communications, the environment is rapidly changing, and the observed fading process is non-stationary. The channel sounder provides a sampled measurement of the continuous CTF $H(t,f)$ that is time-varying and frequency selective. We collect Y = 512 frequency bins across the B = 50 MHz measured bandwidth for each snapshot. The total number of snapshots X = 49536 with a sampling rate of t_s = 975.3 μs. We consider the discrete CTF to be

$$H[m,q] = H(t_s m, f_s q) \tag{9}$$

where the frequency resolution $f_s = B/Y$, the time index $m \in \{0, ..., X-1\}$ and the frequency index $q \in \{0, ..., Y-1\}$

Since the environment changes with a finite rate, we can approximate the fading process to be locally stationary for a region with finite extent in time and frequency. This allows us to locally estimate the power spectral density of the non-WSSUS fading process, in order to describe its TF-varying statistical behavior. This local region is defined by M samples in time and N samples in frequency. Using a sliding window over the recorded CTF, we estimate a discrete version of the TF-dependent LSF in (1). As aforementioned, the observed fading process in vehicular channels shows a much stronger

violation of the WSS assumption than the US. Hence, in this work, we focus on the time variation of the non-stationary fading channel and we assume the channel to be stationary over the whole bandwidth, i.e. $N = Y$. This is in correspondance with previous studies suggesting the stationarity bandwidth to have much larger values in similar scenarios [4].

A. LSF Estimate

Estimating the power spectrum of a process requires statistically independent realizations of the same process, which is very difficult to obtain using measurements. When tapering the measurement data using multiple orthogonal windows, we obtain multiple independent spectral estimates from the same measurement by estimating the spectrum of each individual taper. The total estimated power spectrum is thus calculated by averaging over all tapered spectra.

For the TF-sampled CTF $H[m, q]$, we use the discrete version of the LSF multitaper-based estimator proposed in [15], [25]. The applied orthogonal 2-D tapering windows are computed from K and L orthogonal tapers in time and frequency domains, respectively. We estimate the LSF for consecutive regions in time using a sliding window with the size of $M \times N$ samples in TF domain. The time index of each region $r_t \in \{0, ..., \frac{X-M}{\Delta_t} - 1\}$ corresponds to its center, while Δ_t denotes the sliding time shift between consecutive estimation regions. The LSF estimate is formulated as

$$\hat{C}[r_t, n, p] = \frac{1}{KL} \sum_{w=0}^{KL-1} \left| H^{(G_w)}[r_t, n, p] \right|^2 \tag{10}$$

where $n \in \{0, ..., N-1\}$ denotes the delay index and $p \in \{-M/2, ..., M/2-1\}$ denotes the Doppler index. The tapered spectral estimate $H^{(G_w)}$ is calculated as

$$H^{(G_w)}[r_t, n, p] = \sum_{q'=-N/2}^{N/2-1} \sum_{m'=-M/2}^{M/2-1} G_w[m', q'] \times H[m' + \Delta_t r_t + M/2,\ q' + N/2]\ e^{-j2\pi(pm' - nq')} \tag{11}$$

where the relative time and frequency indexes within each region are m' and q', respectively, and the window functions G_w are localized within the $[-M/2, M/2-1] \times [-N/2, N/2-1]$ region. The tapers are chosen as the discrete prolate spheroidal sequences (DPSS) [35] and the number of used tapers is $K = 3$ and $L = 3$ in both time and frequency domains to balance the noise variance and the square bias [4].

For calculating the stationarity region, we first need to estimate the LSF assuming a minimum stationarity region. While we include the whole bandwidth of $N = Y = 512$ samples, we choose the dimension in time domain $M = 128$ samples corresponding to 124.8 ms. This needs to be validated after we calculate the stationarity time (see Section V); that it is indeed larger than the assumed value. The sliding time shift is selected to be half of the region dimension, i.e. $\Delta_t = 64$ samples. With these parameters, we obtain a LSF estimate every 62.4 ms of delay resolution $\tau_s = 1/B = 20$ ns, and Doppler resolution $\upsilon_s = 1/(Mt_s) = 8$ Hz.

B. CCF and Stationarity Time

The stationarity time can be calculated from the spread of the CCF about the origin in the Doppler lag direction, as shown in (4). We use a discrete time implementation of the CCF in (2), omitting the explicit dependence of CCF on $\Delta\tau$ and only considering the $\Delta\upsilon$ dependence. Hence, the discrete CCF is the 3-D DTFT of the LSF estimate

$$\hat{A}[\Delta m, \Delta q, r_{\Delta\upsilon}] = \mathbf{F}^3\{\hat{C}[r_t, n, p]\} \tag{12}$$

where $\Delta m, \Delta q$ and $r_{\Delta\upsilon}$ are the time lag, frequency lag and Doppler lag indexes, respectively. Similarly, we can write the CCF Doppler moment in discrete form as

$$\hat{s}^{(r_{\Delta\upsilon})} = \frac{1}{\|\hat{A}\|_1} \sum_{r_{\Delta\upsilon}} \sum_{\Delta q} \sum_{\Delta m} |r_{\Delta\upsilon}|\ |\hat{A}[\Delta m, \Delta q, r_{\Delta\upsilon}]| \tag{13}$$

from which the stationarity time can be evaluated based on (5). The bound on LSF variation and the accuracy of approximating LSF to be constant within the stationarity region are provided in [5].

C. Delay and Doppler Spreads

The second-order central moments of the PDP and DPP are of great importance and relevance to fading channels characterization and systems design. They have been usually assumed constant over time. However, the non-stationarity of vehicular channels allows such parameters to be defined only within a local region of stationarity. Therefore, it is reasonable to characterize the delay and Doppler spreads as time-varying channel parameters.

The PDP $\hat{P}$ and DPP $\hat{Q}$ are the projections of the LSF estimate on the delay and Doppler domains, respectively. They can be regarded as the sampled estimate of $P_{\mathbf{TF}}$ and $Q_{\mathbf{TF}}$ from (6). In Fig. 4, the PDP and DPP are depicted for our measurement. From 0 to 35 s, Rx is approaching Tx with an average speed of 40 km/h, which can be seen from the decreasing delay of the LOS in the PDP and the positive Doppler shift of 50 Hz in the DPP. At 35 s, Rx crosses Tx position, resulting in the minimum LOS delay and the Doppler shift from positive to negative 50 Hz. After that, Rx starts to move away from Tx, hence the LOS delay starts to increase again while the Doppler shift remains around negative 50 Hz. Several MPCs can be observed in the profiles. Components from fixed scatterers are showing in the DPP with less power and Doppler shifts between +/- 50 Hz, while short lasting components resulting from moving scatterers in both directions can reach higher positive and negative Doppler shifts.

Based on the estimated profiles, the time-varying RMS delay and Doppler spreads can be calculated, respectively as

$$\hat{\sigma}_\tau[r_t] = \sqrt{\frac{\sum_{n=0}^{N-1} (n\tau_s)^2 \hat{P}[r_t, n]}{\sum_{n=0}^{N-1} \hat{P}[r_t, n]} - \left(\frac{\sum_{n=0}^{N-1} n\tau_s \hat{P}[r_t, n]}{\sum_{n=0}^{N-1} \hat{P}[r_t, n]} \right)^2} \tag{14}$$

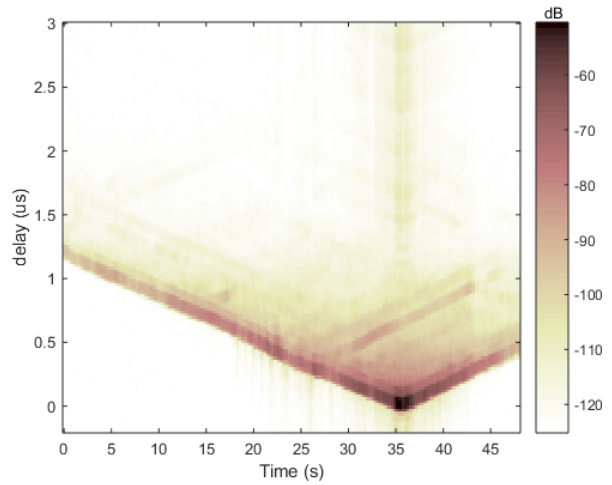

(a)

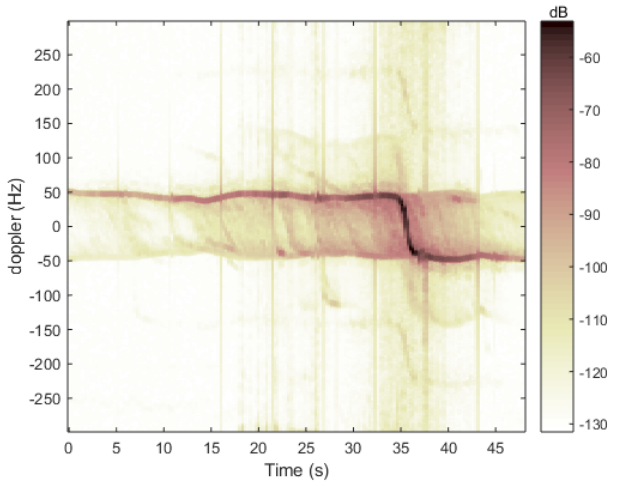

(b)

Fig. 4. Time-varying PDP (a) and DPP (b) for the scenario of crossing Tx position at 35 s with constant speed of 40 km/h

and

$$\hat{\sigma}_{\upsilon}[r_t] = \sqrt{\frac{\sum_{p=-M/2}^{M/2-1} (p\upsilon_s)^2 \hat{Q}[r_t,p]}{\sum_{p=-M/2}^{M/2-1} \hat{Q}[r_t,p]} - \left(\frac{\sum_{p=-M/2}^{M/2-1} p\upsilon_s \hat{Q}[r_t,p]}{\sum_{p=-M/2}^{M/2-1} \hat{Q}[r_t,p]} \right)^2} \tag{15}$$

Before calculating the spreads, pre-processing is carried out separately for each stationarity region. No significant components are found with delay values larger than 3 μs, so we limit the LSF to this value. In order to avoid spurious and noise components, we decide on a power threshold below which we set all the components of the estimated LSF to zero. The threshold is chosen to be 6 dB above the noise level [36].

V. Results and Discussion

A. Stationarity Region

The stationarity region represents the region in time and frequency within which the LSF is highly correlated. Previous studies suggest a stationarity frequency range larger than the measured bandwidth (above 150 MHz according to [4]). Hence, we adopt this result and focus in our analysis on the stationarity time. Based on (12), the LSF correlation can be determined by the CCF spread. Fig. 5 shows the marginal CCF as a function of the Doppler lag, by summing over the other variables. As expected for a correlation function, the CCF is symmetric and has its maximum at the origin. According to (13), the CCF Doppler moment measures the Doppler correlation which is related to the stationarity time T_s as in (5). Based on the calculations done to our measurement data of 48 s, we estimate a stationarity time T_s = 567 ms. This is indeed larger than the assumed minimum value of 124.8 ms used for LSF estimation.

In order to get an intuitive understanding regarding the influence of the scenario, a simpler alternative definition of the stationarity time can be used as $\overline{T}_s = 1/\Delta\upsilon_{max}$, where the maximum Doppler correlation lag $\Delta\upsilon_{max}$ (i.e. the largest $\Delta\upsilon$ for which CCF is effectively nonzero) is used instead of the weighted integral in (4). Consequently, this definition gives a lower bound of T_s in (5) [5]. The violation of WSSUS assumptions can be associated with correlated scatterers corresponding to the same physical object (e.g. building surface). Assuming a maximum angular spread and Doppler shift of the scatterers in our scenario to be $\delta = 4^\circ$ and $\upsilon_{max} = 50$ Hz, respectively, implies $\Delta\upsilon_{max} \approx 2\upsilon_{max}\sin(\delta/2) = 3.49$ Hz [5]. From Fig. 13, the marginal CCF drops to 10% of its peak value at $\Delta\upsilon = 3.9$ Hz, matching well with our assumptions. This yields $\overline{T}_s = 287$ ms $< T_s$. Hence, as the relative speed increases or the scenario changes, e.g. to an urban area with denser scatterers of larger angular spread, the stationarity time is expected to decrease accordingly, which is evident in the results found in [4].

B. LSF Collinearity

Another measure of stationarity that is used in the literature is via the collinearity of LSF [4], [25]. The collinearity is a bounded metric $\in$ [0, 1] that compares different power spectra. First, the collinearity between each two time instances of the LSF is computed for the entire route. Secondly, the local region of stationarity (LRS) is estimated as the time span during which the collinearity exceeds a certain threshold. Being an empirical measure, collinearity results are highly dependent on the selection of the threshold value. Fig. 6 shows the mean LRS calculated from our measurement data versus the applied threshold value. For the mean LRS to have the same value of $T_s = 567$ ms, the threshold is found to be 0.95.

C. Comparing T_s and LRS

While T_s is estimated for the entire route, LRS on the other hand is estimated per time instance. In order to compare both measures, we calculate a local CCF per time instance

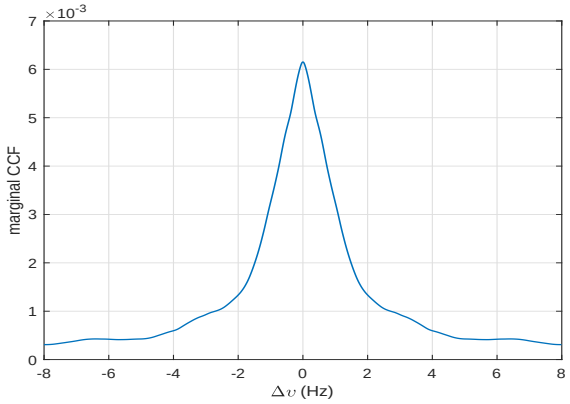

Fig. 5. CCF spread in the Doppler lag direction over the entire route

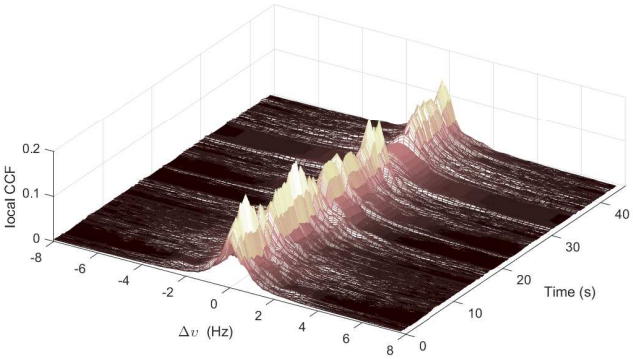

Fig. 7. Local CCF spread in the Doppler lag direction per regions of 1.25 s

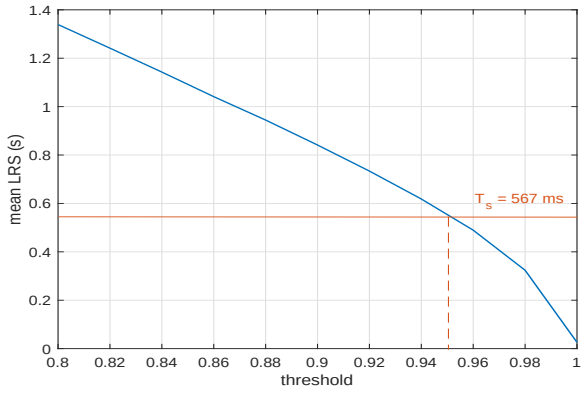

Fig. 6. Mean LRS versus the corresponding threshold applied to the collinearity of LSF

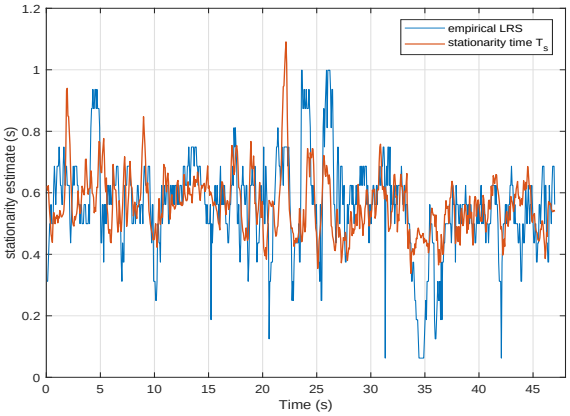

Fig. 8. Stationarity time and LRS for the entire route

over regions of 1.25 s. The local marginal CCF spread in the Doppler lag direction is depicted in Fig. 7 for the entire route. Notice the increase in the CCF spread around the time Rx crosses Tx position (35 s), indicating a smaller stationarity time. Fig. 8 compares T_s and LRS with 0.95 threshold value over the entire route. The minimum values of T_s and LRS are 337 ms and 62.42 ms, respectively. Although some correlation can be observed between the two metrics (Pearson correlation coefficient of 0.37), the variance of T_s around the mean value is smaller compared to LRS (0.009 and 0.024, respectively). This is indeed expected; the stationarity time T_s characterizes the entire propagation environment, which does not change much on a time instance basis. Another difference between the two metrics is that LRS values are discrete, confined only to multiples of the minimum time difference between instances of the LSF, while T_s can take any value. Hence, we conclude that the stationarity time T_s based on the CCF gives a more accurate characterization of the channel.

D. Delay and Doppler Spreads Evaluation and Statistical Modeling

For the non-stationary channel, the fading parameters can be accurately evaluated within each staionarity region, so that the channel modeling becomes physically meaningful. Based on our estimation of the staionarity time, the corresponding number of samples in time domain is $M = 580$ samples. Hence, the LSF estimate is recomputed using a sliding time shift of half the stationarity region dimension.

The PDP and DPP are depicted in Fig. 4, while the corresponding RMS delay and Doppler spreads from (14, 15) are in Fig. 9. The two parameters are showing quite similar behaviors, indicating a high correlation between both spreads. The Pearson correlation coefficient is calculated as 0.45 over the entire route. The mean of the spread values (48.91 ns and 11.82 Hz) are much smaller than typical values in cellular scenarios (0.1-10 μs) due to the dominant LOS condition [2]. Limited studies of vehicular channels in the 2 GHz band are found in the literature. The work in [37] reports a delay spread of 102 ns in an urban T-intersection for obstructed LOS, and 53 ns in an expressway LOS scenario at 2.4 GHz. However, it is not mentioned what are the mean values or the statistics found. The V2V channel is characterized in an urban environment in [17] at 2.3 and 5.25 GHz. It shows that the mean delay spread slightly decreases at the higher frequency (33.3 ns to 28.3 ns), which can be considered insignificant. In the 5 GHz band, several studies in similar scenarios report mean delay spread values that are in the same range of our results (e.g. 40-50 ns in [26], 45 ns in [27], 47 ns in [30] and

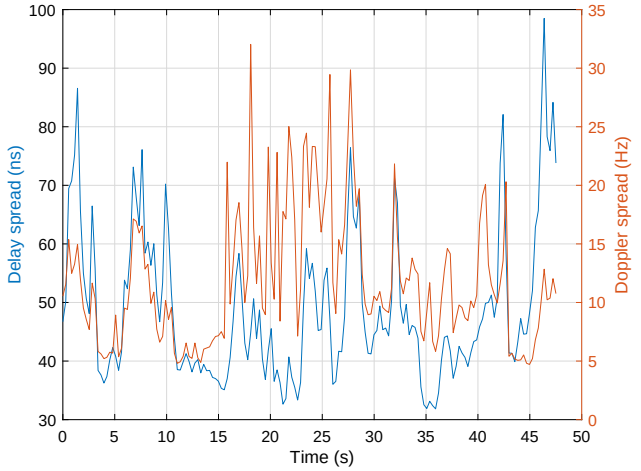

Fig. 9. Time-varying RMS delay and Doppler spreads of the crossing scenario with constant speed of 40 km/h

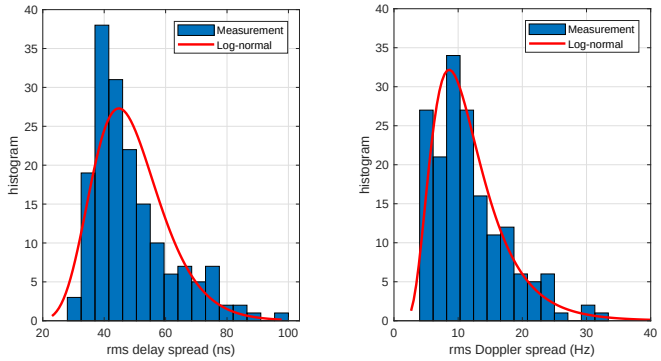

(a) (b)

Fig. 10. Histograms of the (a) RMS delay spread and (b) RMS Doppler spread and the corresponding lognormal models for the entire route

35.8 ns in [28]). As reported in [26], other vehicles driving beside Tx and Rx may not represent relevant scatterers. This is because the placement of the antennas in our setup is slightly above the other vehicles. Large scattering objects such as trucks, buildings or metallic structures constitute more relevant MPCs.

In order to statistically characterize the spreads over the entire route, we use the Kolmogorov-Smirnov (KS) test [38] to select the distribution by comparing the p-value of different models: lognormal, normal, Nakagami, Rayleigh, Weibull, and Rician. It is found that the lognormal distribution gives the best fit to the measured parameters among the candidate models. Fig. 10 shows the histograms of the RMS delay and Doppler spreads and their corresponding best fit models. Table II summarizes the details of the lognormal distribution for both parameters. We also include the maxima of the spreads, as they represent critical values for communication systems.

A measure of the channel selectivity that is directly related to the delay and Doppler spreads is the coherence region. T_c and F_c are calculated from the maximum RMS Doppler spread and delay spread, respectively, according to (7). Based on our measurements, we obtain $T_c = 4.97$ ms and $F_c = 1.62$ MHz. This results in a coherence region $T_cF_c \approx 8{\times}10^3 \gg 1$ indicating that the channel is dispersion-underspread. In order to verify the other part of the inequality in (8), we need to calculate the stationary region. We use the estimated stationarity time $T_s = 567$ ms, while for the stationarity bandwidth, we adopt the minimum value of $F_s = 150$ MHz reported for similar scenarios in [4]. Hence, the stationarity region is considered to be $T_sF_s \approx 8.5{\times}10^7$, verifying that the channel is indeed DU.

E. Application Relevance

The assumptions of WSSUS fading channel have lead to simplification of transceivers design, simulation, and evaluation of many communication systems. Long-term channel properties are evaluated and assumed stationary, while dispersions are regarded as results of uncorrelated scatterers.

TABLE II
STATISTICS OF THE RMS DELAY AND DOPPLER SPREADS LOG-NORMAL DISTRIBUTIONS

	Mean	Max.	KS-test p-value	μ	σ
$\hat{\sigma}_\tau$	48.91 ns	98.49 ns	0.092	3.86	0.24
$\hat{\sigma}_\upsilon$	11.82 Hz	32.03 Hz	0.722	2.36	0.46

Unfortunately, practical channels, specially in vehicular communications, do not satisfy these assumptions; this influences the performance of such systems. For example, the gain of transmission methods utilizing adaptive modulation, channel coding, diversity in time, frequency, delay or Doppler is limited by the amount of correlation in each domain of the channel [39], [40]. In this section, we briefly discuss the relevance of the non-stationarity characterization to some practical aspects as suggested in [5].

1) Ergodic Capacity: It is well known that in order to achieve ergodic capacity, a very long Gaussian codebook is required, where the length is dependent on the dynamics of the fading process. In particular, it must be long enough for the fading to reflect its ergodic nature, i.e. the coding should cover numerous independent identically distributed (i.i.d.) fading realizations [31]. This can be formulated as

$$C_{erg} = \mathrm{E}[B\ \log_2(1+\gamma)] = \int B\ \log_2(1+\gamma)P(\gamma)\ \mathrm{d}\gamma \quad (16)$$

where γ is the instantaneous SNR with the channel state perfectly known to Rx. Whether sufficient averaging can be achieved for this equality to hold depends on the number of i.i.d. fading coefficients offered by the channel.

For doubly selective channels, independent fading coefficients are obtained every T_c in time and F_c in frequency, and the fading statistics remain constant over a region of T_sF_s. Hence, the value $N_i = T_sF_s/(T_cF_c)$ approximately characterizes the number of i.i.d. fading coefficients offered by the channel. For the WSSUS channels, $T_sF_s \to \infty$ so that N_i is large enough and C_{erg} can be achieved. However, as the stationarity region decreases, C_{erg} can only be defined for sufficiently large N_i. It is important to note that the value of N_i changes across different stationarity regions due to the

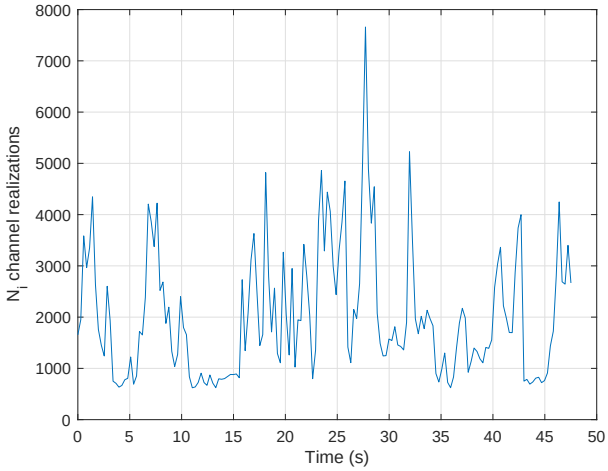

Fig. 11. Number of i.i.d. channel realizations per stationarity region across the entire route

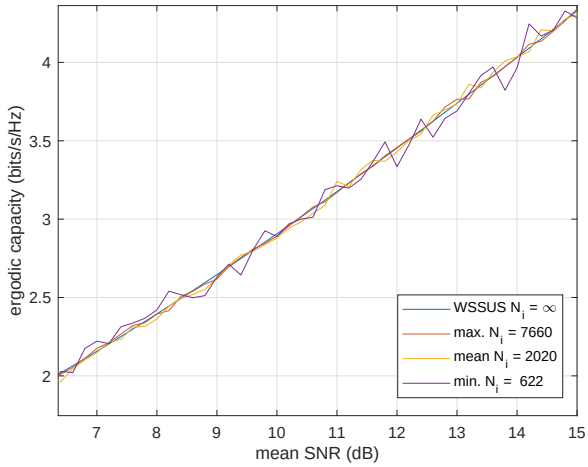

Fig. 12. Channel capacity averaged over different N_i values for several SNRs using i.i.d. Rayleigh coefficients

TABLE III
RELATIVE ERROR (RE) BETWEEN THE CAPACITY FOR SEVERAL N_i VALUES AND THE WSSUS CHANNEL

	WSSUS	Min.	Mean	Max.
N_i	∞	622	2020	7660
RE (%)	0	2.15	1.23	0.63

variation of the size of the coherence region. Based on our measurement, Fig. 11 shows the value of N_i across different regions of stationarity in time.

In order to illustrate the (in-)validity of the ergodic assumption for this channel, we simply calculate the capacity of a Rayleigh fading channel using different values of N_i. Fig. 12 shows the capacity versus mean SNR by averaging over the maximum, mean and minimum values of N_i based on our measurements. We compare these to the WSSUS channel ($N_i \to \infty$). Table III lists the relative error of the capacity between each case and the WSSUS channel. These results indicate that the channel may not support coding schemes with enough averaging for the validity of the ergodic capacity. Such scenarios can then be characterized using the outage capacity [31]. Unlike the ergodic scenario, schemes designed to achieve outage capacity allow for channel errors. The capacity-versus-outage performance is determined by the probability that the channel cannot support a given rate, i.e. an outage probability is associated to any given rate.

2) Fading Mitigation: The stationarity and correlation parameters influence the limitations of transmission schemes that use the long-term properties and selectivity of the channel to combat fading. For example, diversity techniques essentially aim at providing Rx with multiple independently faded replicas of the signal. It is evident that diversity gain improves monotonically with increasing the number of i.i.d. channel realizations. In fact, as the number $\to \infty$, the performance of coherent diversity reception converges to the performance over a non-fading AWGN channel [40]. The dispersive wireless channel has inherent diversity that can be exploited with appropriate schemes. Common techniques include time diversity, frequency diversity, delay diversity and Doppler diversity, as well as joint diversity between several domains [39].

Interleaving over several coherence times, often used with error correction coding, is a form of time diversity. With the vehicular channel being non-stationary, the effective gain achieved will change depending on the varying coherence parameters of the channel. For the multipath-Doppler RAKE receivers [40], the amount of diversity order achievable will be limited by the amount of delay and Doppler correlation in the channel. In addition, the variation of delay and Doppler spreads will result in a varying effective diversity for the non-stationary channel. Hence, the joint knowledge of stationarity and coherence/spread parameters and their statistical behavior can be employed to improve the performance of such methods.

In order to quantify the influence of the non-stationarity assumption on the effective diversity, we consider the maximum achievable diversity order of time, frequency, Doppler and delay diversities, with the diversity orders given respectively as

$$\begin{aligned} d_t &= \frac{T_s}{T_c}, \qquad d_f = \frac{F_s}{F_c}, \\ d_\upsilon &= \frac{\sigma_\upsilon}{s_{\mathbf{TF}}^{(\Delta\upsilon)}}, \quad d_\tau = \frac{\sigma_\tau}{s_{\mathbf{TF}}^{(\Delta\tau)}}. \end{aligned} \tag{17}$$

Fig. 13 shows the effective diversity orders across different regions of stationarity based on our measurement, where the delay correlation $s_{\mathbf{TF}}^{(\Delta\tau)}$ is calculated from the stationarity bandwidth value of 150 MHz. Since the diversity orders are proportional to the RMS delay and Doppler spreads with only a scaling factor as in (17), their statistical distribution should follow a lognormal model as well. Note that the use of the maximum excess spread instead of the RMS spread for the calculation of the delay and Doppler diversity orders would result in higher values than depicted in Fig. 13.

VI. CONCLUSION

In this paper, the non-stationary fading process of vehicular channels is analyzed based on V2I channel measurements at

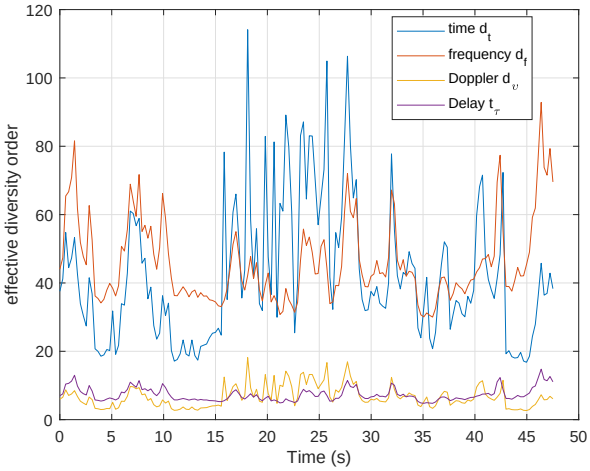

Fig. 13. Effective diversity order of several techniques per stationarity region across the entire route

1.35 GHz in a suburban environment. We apply the framework of the local scattering function (LSF) and channel correlation function to characterize the stationarity time and find it to be more accurate than the empirical collinearity estimate. A stationarity time of 567 ms is calculated for the crossing scenario at 40 km/h speed. Based on the LSF, time-varying delay and Doppler power profiles are obtained and used to calculate the corresponding second-order central moments. The empirical distribution of the RMS delay spread and Doppler spread is best fitted by a lognormal model. Finally, practical relevance of the non-stationarity of the channel is briefly discussed. Results show that as the assumption of WSSUS is violated, the assumption of ergodic capacity and its application becomes unreliable. Moreover, the gain of the effective diversity varies with the stationarity and coherence parameters of the channel. Hence, the optimal performance of communication systems can be obtained by considering the varying nature of such parameters via adaptive schemes.

REFERENCES

[1] Intelligent Transport Systems (ITS); Vehicular Communications; Basic Set of Applications; Definitions, ETSI TR 102 638 V1.1.1, Tech. Rep., 2009.

[2] A. F. Molisch, F. Tufvesson, J. Karedal, and C. F. Mecklenbrauker, "A survey on vehicle-to-vehicle propagation channels," *IEEE Wireless Communications*, vol. 16, no. 6, pp. 12–22, 2009.

[3] C. F. Mecklenbrauker, A. F. Molisch, J. Karedal, F. Tufvesson, A. Paier, L. Bernadó, T. Zemen, O. Klemp, and N. Czink, "Vehicular channel characterization and its implications for wireless system design and performance," *Proceedings of the IEEE*, vol. 99, no. 7, pp. 1189–1212, 2011.

[4] L. Bernadó, T. Zemen, F. Tufvesson, A. F. Molisch, and C. F. Mecklenbräuker, "The (in-) validity of the WSSUS assumption in vehicular radio channels." in *23rd IEEE International Symposium on Personal, Indoor and Mobile Radio Communications, PIMRC*, 2012, pp. 1757–1762.

[5] G. Matz, "On non-WSSUS wireless fading channels," *IEEE Transactions on Wireless Communications*, vol. 4, no. 5, pp. 2465–2478, 2005.

[6] A. Paier, J. Karedal, N. Czink, H. Hofstetter, C. Dumard, T. Zemen, F. Tufvesson, A. F. Molisch, and C. F. Mecklenbrauker, "Car-to-car radio channel measurements at 5 GHz: Pathloss, power-delay profile, and delay-Doppler spectrum," in *2007 4th International Symposium on Wireless Communication Systems*. IEEE, 2007, pp. 224–228.

[7] P. Fan, J. Zhao, and I. Chih-Lin, "5G high mobility wireless communications: Challenges and solutions," *China Communications*, vol. 13, no. 2, pp. 1–13.

[8] P. Bello, "Characterization of randomly time-variant linear channels," *IEEE transactions on Communications Systems*, vol. 11, no. 4, pp. 360–393, 1963.

[9] G. Acosta-Marum and M. A. Ingram, "A BER-based partitioned model for a 2.4 GHz vehicle-to-vehicle expressway channel," *Wireless Personal Communications*, vol. 37, no. 3-4, pp. 421–443, 2006.

[10] D. W. Matolak, "Channel modeling for vehicle-to-vehicle communications," *IEEE Communications Magazine*, vol. 46, no. 5, 2008.

[11] I. Sen and D. W. Matolak, "Vehicle-to-vehicle channel models for the 5-GHz band," *IEEE Transactions on Intelligent Transportation Systems*, vol. 9, no. 2, pp. 235–245, 2008.

[12] R. He, O. Renaudin, V.-M. Kolmonen, K. Haneda, Z. Zhong, B. Ai, and C. Oestges, "A dynamic wideband directional channel model for vehicle-to-vehicle communications," *IEEE Transactions on Industrial Electronics*, vol. 62, no. 12, pp. 7870–7882, 2015.

[13] Y. Yuan, C.-X. Wang, Y. He, M. M. Alwakeel *et al.*, "3D wideband non-stationary geometry-based stochastic models for non-isotropic MIMO vehicle-to-vehicle channels," *IEEE Transactions on Wireless Communications*, vol. 14, no. 12, pp. 6883–6895, 2015.

[14] R. He, B. Ai, G. L. Stüber, and Z. Zhong, "Mobility model-based non-stationary mobile-to-mobile channel modeling," *IEEE Transactions on Wireless Communications*, vol. 17, no. 7, pp. 4388–4400, 2018.

[15] G. Matz, "Doubly underspread non-WSSUS channels: Analysis and estimation of channel statistics," in *4th IEEE Workshop on Signal Processing Advances in Wireless Communications, SPAWC*. IEEE, 2003, pp. 190–194.

[16] M. Gudmundson, "Correlation model for shadow fading in mobile radio systems," *Electronics letters*, vol. 27, no. 23, pp. 2145–2146, 1991.

[17] A. Roivainen, P. Jayasinghe, J. Meinila, V. Hovinen, and M. Latva-aho, "Vehicle-to-vehicle radio channel characterization in urban environment at 2.3 GHz and 5.25 GHz," in *2014 IEEE 25th Annual International Symposium on Personal, Indoor, and Mobile Radio Communication (PIMRC)*. IEEE, 2014, pp. 63–67.

[18] M. Herdin, N. Czink, H. Ozcelik, and E. Bonek, "Correlation matrix distance, a meaningful measure for evaluation of non-stationary MIMO channels," in *61st IEEE Vehicular Technology Conference, VTC*. IEEE, 2005, pp. 136–140.

[19] O. Renaudin, V.-M. Kolmonen, P. Vainikainen, and C. Oestges, "Non-stationary narrowband MIMO inter-vehicle channel characterization in the 5-GHz band," *IEEE Transactions on Vehicular Technology*, vol. 59, no. 4, pp. 2007–2015, 2010.

[20] L. Bernadó, T. Zemen, A. Paier, G. Matz, J. Kåredal, N. Czink, C. Dumard, F. Tufvesson, M. Hagenauer, A. Molisch *et al.*, "Non-WSSUS vehicular channel characterization at 5.2 GHz spectral divergence and time-variant coherence parameters," in *XXIXth URSI General Assembly 2008*, 2008.

[21] R. He, O. Renaudin, V.-M. Kolmonen, K. Haneda, Z. Zhong, B. Ai, and C. Oestges, "Characterization of quasi-stationarity regions for vehicle-to-vehicle radio channels," *IEEE Transactions on Antennas and Propagation*, vol. 63, no. 5, pp. 2237–2251, 2015.

[22] D. Umansky and M. Patzold, "Stationarity test for wireless communication channels," in *Global Telecommunications Conference, GLOBECOM*. IEEE, 2009, pp. 1–6.

[23] T. J. Willink, "Wide-sense stationarity of mobile MIMO radio channels," *IEEE Transactions on Vehicular Technology*, vol. 57, no. 2, pp. 704–714, 2008.

[24] A. Gehring, M. Steinbauer, I. Gaspard, and M. Grigat, "Empirical channel stationarity in urban environments," in *Proc. Eur. Personal Mobile Communications Conf. (EPMCC), Vienna, Austria*, 2001.

[25] A. Paier, T. Zemen, L. Bernado, G. Matz, J. Kåredal, N. Czink, C. Dumard, F. Tufvesson, A. Molisch, and C. Mecklenbräuker, "Non-WSSUS vehicular channel characterization in highway and urban scenarios at 5.2 GHz using the local scattering function," in *International Workshop on Smart Antennas (WSA)*, 2008, pp. 9–15.

[26] L. Bernado, T. Zemen, F. Tufvesson, A. F. Molisch, and C. F. Mecklenbräuker, "Delay and Doppler spreads of nonstationary vehicular channels for safety-relevant scenarios," *IEEE Transactions on Vehicular Technology*, vol. 63, no. 1, pp. 82–93, 2014.

[27] R. He, A. F. Molisch, F. Tufvesson, Z. Zhong, B. Ai, and T. Zhang, "Vehicle-to-vehicle propagation models with large vehicle obstructions," *IEEE Transactions on Intelligent Transportation Systems*, vol. 15, no. 5, pp. 2237–2248, 2014.

[28] R. He, O. Renaudin, V.-M. Kolmonen, K. Haneda, Z. Zhong, B. Ai, S. Hubert, and C. Oestges, "Vehicle-to-vehicle radio channel characterization in crossroad scenarios." *IEEE Trans. Vehicular Technology*, vol. 65, no. 8, pp. 5850–5861, 2016.

[29] Y. Shui, F. Li, J. Yu, W. Chen, C. Li, K. Yang, and F. Chang, "Vehicle-to-vehicle radio channel characteristics for congestion scenario in dense urban region at 5.9 GHz," *International Journal of Antennas and Propagation*, vol. 2018, 2018.

[30] J. Kunisch and J. Pamp, "Wideband car-to-car radio channel measurements and model at 5.9 GHz," in *Vehicular Technology Conference, 2008. VTC 2008-Fall. IEEE 68th*. IEEE, 2008, pp. 1–5.

[31] E. Biglieri, J. Proakis, and S. Shamai, "Fading channels: Information-theoretic and communications aspects," *IEEE Transactions on Information Theory*, vol. 44, no. 6, pp. 2619–2692, 1998.

[32] P. Laly, D. P. Gaillot, M. Liénard, P. Degauque, E. Tanghe, W. Joseph, and L. Martens, "Flexible real-time MIMO channel sounder for multi-dimensional polarimetric parameter estimation," in *IEEE Conference on Antenna Measurements & Applications (CAMA)*. IEEE, 2015, pp. 1–3.

[33] "Technical specification group radio access network; vehicle-to-everything (V2X) services based on LTE; user equipment (UE) radio transmission and reception. TR 36.786 v14.0.0," 3GPP, Tech. Rep., 2017.

[34] B. H. Fleury, "An uncertainty relation for WSS processes and its application to WSSUS systems," *IEEE Transactions on Communications*, vol. 44, no. 12, pp. 1632–1634, 1996.

[35] D. Slepian and H. O. Pollak, "Prolate spheroidal wave functions, Fourier analysis and uncertaintyi," *Bell System Technical Journal*, vol. 40, no. 1, pp. 43–63, 1961.

[36] A. F. Molisch and M. Steinbauer, "Condensed parameters for characterizing wideband mobile radio channels," *International Journal of Wireless Information Networks*, vol. 6, no. 3, pp. 133–154, 1999.

[37] G. Acosta, K. Tokuda, and M. A. Ingram, "Measured joint doppler-delay power profiles for vehicle-to-vehicle communications at 2.4 GHz," in *IEEE Global Telecommunications Conference, 2004. GLOBECOM'04.*, vol. 6. IEEE, 2004, pp. 3813–3817.

[38] F. J. Massey Jr, "The Kolmogorov-Smirnov test for goodness of fit," *Journal of the American statistical Association*, vol. 46, no. 253, pp. 68–78, 1951.

[39] B. Sklar, "Rayleigh fading channels in mobile digital communication systems part II: Mitigation," *IEEE Communications Magazine*, vol. 35, no. 9, pp. 148–155, Sept 1997.

[40] A. M. Sayeed and B. Aazhang, "Joint multipath-Doppler diversity in mobile wireless communications," *IEEE Transactions on Communications*, vol. 47, no. 1, pp. 123–132, 1999.

Marwan Yusuf received the M. Sc. degree in Electrical Engineering from Istanbul Medipol University (Turkey) in 2016 where he was a Research Assistant in the Communications, Signal Processing, and Networking Center (CoSiNC). His scientific work focused on physical layer security for wireless channels. Since January 2018, he has been a Doctoral Researcher in the Department of Information Technology at Ghent University, Belgium (IMEC-UGent/INTEC) where he works on measurement-based modelling of indoor and outdoor wireless propagation with emphasis on vehicular communication channels.

Emmeric Tanghe was born in Tielt, Belgium, on August 31, 1982. He received the M. Sc. degree in Electrical Engineering from Ghent University (Ghent, Belgium) in 2005 and the Ph. D. degree in electrical engineering from the same institution in 2011. From September 2005 until May 2011, he was a Research Assistant with the Department of Information Technology at Ghent University (imec-UGent/INTEC). His scientific work focused on the modeling of indoor and outdoor propagation through field measurements. Since May 2011, he has been a Postdoctoral Researcher with the same institution and continues his work in propagation modeling. From October 2012 until September 2018, he was a Postdoctoral Fellow of the FWO-V (Research Foundation - Flanders). In October 2015 he became a part-time professor in medical applications of electromagnetic fields in and around the human body.

Frédéric Challita received the B.S. degree in Electronic Information and Telecommunication from Lebanese University (ULFG), Roumyeh, Lebanon, in 2015, and the masters degree in Microtechnologies and Systems Architectures and Networks from Telecom Bretagne, Brest, France, in 2016. Since October 2016, He is a Ph.D. student at the Institute of Electronics, Microelectronics, and Nanotechnology (IEMN), group TELICE in Villeneuve dAscq, France. His research interests include the characterization and modeling of massive MIMO radio channels from the mobile telecommunications frequency range to the millimeter frequency range. In particular, he focuses on the development of antenna selection strategies and signal processing techniques under the massive MIMO framework to optimize the resource allocation in terms of capacity to distributed users.

Pierre Laly is an engineer of study. His main current areas of research are the study, design and production of electronic cards to build prototypes dedicated to digital and/or analog telecommunications. He realizes the implementation and programming of microcontrollers, DSP, CPLD, FPGA components and the study and the realization of sub systems for the recovery and the statistical treatment of the information of the various prototypes.

Davy P. Gaillot received the B.S. degree in mechanical engineering from Ecole Nationale dIngnieurs de Metz (ENIM), Metz, France, in 2002, and the masters degree in mechanics, materials, structures, and processes from the University of Metz, Metz, France. He also received the Ph.D. degree, in 2007, from the Department of Materials Science and Engineering at the Georgia Institute of Technology, Atlanta, GA, USA. He was a Postdoctoral Fellow at the Institute of Electronics, Microelectronics, and Nanotechnology (IEMN) in Villeneuve dAscq, France. Since 2008, he has been an Associate Professor at the University of Lille 1 in the IEMNTELICE Group and recently also joined the Institute of Research in Software and Hardware Components for Information and Advanced Communications (IRCICA). His research activities include radio-communications, propagation, channel modeling and experimental channel sounding from the wireless telecommunications frequency range to THz. He currently is one of the French substitute delegates and active participant for the European COST action CA15105 IRACON (Incluse Radio Communications Networks for 5G and Beyond).

Martine Lienard received the Ph.D. degree from the University of Lille, Lille, France, in 1993. Since 1990, she has been with the Telecommunications, Interferences and Electromagnetic Compatibility (TELICE) group of the Institute of Electronic, Microelectronic and Nanotechnology (IEMN) of University of Lille. She is currently a Professor at University of Lille and Head of the TELICE Group. Her current research deals with mobile localization techniques in non cooperative mode and theoretical and experimental channel characterization in complex environment. She is also involved in challenges of MIMO and Massive MIMO techniques, mainly dedicated for communication in rail and road transportation systems and industry 4.0.

Luc Martens received the M.Sc. degree in electrical engineering from the Ghent University, Belgium in July 1986. From September 1986 to December 1990 he was a research assistant at the Department of Information Technology (INTEC) of the same university. During this period, his scientific work was focused on the physical aspects of hyperthermic cancer therapy. His research work dealt with electromagnetic and thermal modelling and with the development of measurement systems for that application. This work led to the Ph.D. degree in December 1990. Since 1991, he manages the WAVES research group at INTEC. This group is since 2004 part of the iMinds institute and since April 1993 he is Professor at Ghent University. His experience and current interests are in modelling and measurement of electromagnetic channels, of electromagnetic exposure e.g. around telecommunication networks and systems such as cellular base station antennas, and of energy consumption in wireless networks. He is author or co-author of more than 300 publications in the domain of electromagnetic channel predictions, dosimetry, exposure systems and health and wireless communications.

Wout Joseph was born in Ostend, Belgium on October 21, 1977. He received the M. Sc. degree in electrical engineering from Ghent University (Belgium), in July 2000. From September 2000 to March 2005 he was a research assistant at the Department of Information Technology (INTEC) of the same university. During this period, his scientific work was focused on electromagnetic exposure assessment. His research work dealt with measuring and modelling of electromagnetic fields around base stations for mobile communications related to the health effects of the exposure to electromagnetic radiation. This work led to a Ph. D. degree in March 2005. From April 2005-2009, he was postdoctoral researcher for iMinds-UGent/INTEC. From October 2007 to October 2013, he was a Post-Doctoral Fellow of the FWO-V (Research Foundation Flanders). Since October 2009, he is professor in the domain of Experimental Characterization of wireless communication systems. He is IMEC PI since 2017. His professional interests are electromagnetic field exposure assessment, in-body electromagnetic field modelling, electromagnetic medical applications, propagation for wireless communication systems, IoT, antennas and calibration. Furthermore, he specializes in wireless performance analysis and Quality of Experience.